ECS Transactions, 66 (9) 17-27 (2015)
10.1149/06609.0017ecst ©The Electrochemical Society

Conductive Additive for Si/Mesoporous Carbon Anode for Li-Ion Batteries: Commercial Graphite vs Super C65

Arlavinda Rezqita [a,b], Raad Hamid[a], Sabine Schwarz[c], Hermann Kronberger[b], Atanaska Trifonova[a]

[a] Mobility Department, AIT Austrian Institute of Technology GmbH, Vienna 1210, Austria
[b] Institute of Chemical Technologies and Analytics, Vienna University of Technology, Vienna 1060, Austria
[c] University Service Centre for Transmission Electron Microscopy, Vienna University of Technology, Vienna A-1040, Austria

Silicon is a promising candidate for anodes in lithium-ion batteries (LIB) due to its high theoretical capacity. However, Si has low electrical conductivity (theoretical: 6.7 x 10^{-4} S cm^{-1}). Proper conductive additive is needed in order to improve the electrical conductivity of Si-based anodes. Here we focus on applying two commercial conductive addictives: graphite and carbon black Super C65 for silicon-mesoporous carbon (Si/MC) composite anodes. The structure and morphology of the electrodes were characterized by nitrogen adsorption, scanning electron microscopy (SEM), and focus ion beam/transmission electron microscopy (FIB/TEM). Furthermore, the electrochemical performance of the electrodes was characterized by cyclic voltammetry, galvanostatic charge/discharge tests, and impedance spectroscopy. In principles, our work could be effective for the choice of conductive additives to improve the electrical performance of Si/MC anodes.

1. Introduction

Increasing the energy density of LIB requires the development of new electrode materials with higher charge capacities.[1] In anode side, silicon has attracted interest for LIB due to its high theoretical capacity of 3579 mAh g^{-1}.[2] However, practical application is limited because of its poor cycling stability. The large volume changes of Si anodes during alloying/dealloying with lithium cause loss of electrical contact between Si particles and current collector.[3,4] It leads to increasing internal resistance and degradation of the electrode. To improve the cycling stability of the electrode, continuous electrical conducting pathways and stable solid-electrolyte interphases (SEI) are required. In this case, conductive additives play important role to improve the conductive percolation network of the Si-based anodes. Carbon materials are selected as conductive additives due to their high conductivity.[5] They are nontoxic and environmentally benign. In addition, carbon coatings on Si electrodes have been reported to modify the SEI morphology which shorten the lithium ion diffusion path.[6] Si anodes with various conductive carbon materials such as carbon black (CB),[7] graphite,[8] graphene, [9–11] carbon nanotubes (CNTs),[12,13] multiwalled carbon nanotubes (MWCNT),[14] and carbon

nanofibers (CNFs),[15] have shown better electrochemical performance than pure Si anodes.

To increase the conductivity of electrodes, two strategies have been widely adopted: (i) doping and coating of conductive phases to improve the intrinsic conductivity of active materials; and (ii) incorporation of conductive additives into the electrodes to form conductive networks around the active materials. Among a variety of carbon materials, CB and graphite are the most popular conductive additive because of their low cost, high electrical conductivity, and closer to commercialization for LIB full cells. In general, carbon black has a spherical shape with a relatively high specific surface area (SSA), whereas graphite has a platelet-like shape with a lower SSA. SSA increases in inverse proportion to the particle size. Although smaller particle size of CB improves the rate of lithiation/delithiation and fracture resistance, it offers a large surface area for electrolyte-reduction reactions for SEI formation. In consequence, the irreversible loss of lithium at first cycle is higher. The morphological structure of conductive additive also influences the mechanical stability and porosity of the total electrode.

In this work, the effects of commercial graphite and carbon black Super C65 on the performance of the as-synthesized Si/MC composite anodes were comparatively studied. Mesoporous carbon matrices in the Si/MC composites were derived from carbonization of Resorcinol-Formaldehyde aerogel. They were micrometer sized which might lead to large interparticle contact resistance. Therefore, smaller sized carboneous material were needed to improve the interparticle contact. The diffusion of lithium ions in both electrodes was further discussed.

2. Experimental

The active material was synthesized by dispersing SiNP with a particle size of 30-50 nm (Nanostructured and Amorphous Materials Inc., USA) into Resorcinol-Formaldehyde (RF) gel. Resorcinol (Merck KGaA) 0.29 M and Formaldehyde solution (Merck Schuchardt) 0.57 M were used for preparing the RF gel. The pH value was adjusted in the range of 6.5 – 7.4 by adding NH_3 (Carl Path GmbH) 5% in H_2O. The dried Si/RF was calcined at 650°C for 10 h under flowing Argon (Ar) to yield Si/MC composites. The obtained powders were immersed in an HF (1M) solution for 1 h. Then the powders were filtered and rinsed off with distilled water to remove any residual HF and dried in an oven at 120°C for 24 h in air. The conductive Graphite and Super C65 we investigated were provided by MTI Corporation. The electrodes were prepared with the Si/MC composites (75 wt%), conductive additive (15%), polyacrylic acid (PAA, 10 wt%) and dissolved in N-methyl-2-2pyrrolidinone (NMP). The slurry was coated onto copper foil and dried at room temperature. The electrodes with a 15 mm diameter were dried at 60°C for 2h and 120°C for 4h under vacuum and pressed between two hot stainless steels rollers at 120°C. 2032 type coin cells were then assembled in an Ar filled dry box using foils of Li metal as reference electrodes and Freundberger separators saturated with 1M LiPF6 in (1:1 wt/wt, EC:DMC).

The structure of the synthesized Si/MC composite, Super C65, and conductive graphite was determined by X-ray diffraction (XRD, using an X´PERT (PRO) POWDER – Panalytical X-ray diffractometer) with Cu-Kα radiation (λ = 1.5418Å).

Surface area and pore diameter were analysed by Brunauer-Emmett-Teller (BET) test and Barrett−Joyner−Halenda (BJH), respectively, using a Quantachrome Instruments Autosorb iQ, US. The morphology and the size of particles were observed by a Scanning Electron Microscope (SEM, FEI/Philips XL-30 Field Emission ESEM) with an energy dispersive spectroscopy (EDS) detector and Transmission Electron Microscopy (TEM, FEI Tecnai). A thin cross-section of the electrode was prepared by Focused Ion Beam (FIB).

For the electrochemical properties of the electrodes, cyclic voltammetry (CV) and the charge/discharge (C/D) tests were conducted on a Maccor Series 4000 battery tester at room temperature. CV measurements were done at a scan rate of 20 μVs^{-1} over the potential window of 0.01–1V versus Li/Li^{+}. The charge/discharge (C/D) tests were carried out with a constant-current-constant voltage (CCCV) mode within the voltage range from 0.01 to 1 V at a constant current density of 1C. Electrochemical Impedance Spectroscopy (EIS) tests were measured by VersaSTAT MC Princeton Applied Research with the frequency range between 500 kHz to 1 Hz and the applied AC voltage 10 mV. All the electrochemical tests were performed at room temperature.

3. Results and Discussion

X-Ray diffractograms of the two carbon samples (Super C65 and Conductive Graphite) are compared in Figure 1. The XRD pattern of the conductive graphite exhibits peaks at 25.6°, 44.2°, and 52.8°, which correspond to planes (002), (011), and (004), respectively, whereas the XRD pattern of Super C65 features broad peaks at 24° and 44.2°, which correspond to (002) and (011) planes, respectively.[16] The presence of a broad peak at 24°, instead of a narrow diffraction peak, is associated with the disordered structure. Conductive graphite has an ABABAB stacking arrangement, while Super C65 has random rotations and translations as characteristic of turbostratic disorder. The degree of crystallinity was proven to influence the capacity, kinetics, and the first cycle irreversible capacity loss.[17]

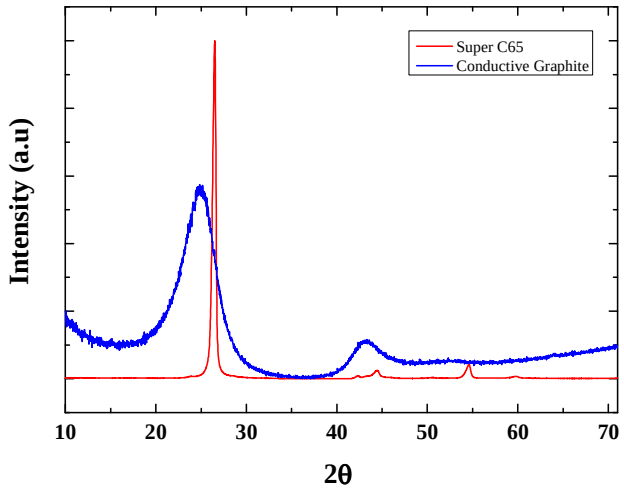

Figure 1. XRD patterns of Super C65 and Conductive Graphite

The physicochemical properties of Super C65 and conductive graphite were measured and presented in TABLE I. The BET measurement shows that the SSA of Super C65 (62.062 $m^2 g^{-1}$) is higher than that of graphite (16.531 $m^2 g^{-1}$). According to the BJH calculation the pore diameters were 2.735 and 0.879 nm, for Super C65 and conductive graphite, respectively. Super C65 has a size distribution that peaks at ~70 μm with a size 0.2 – 600 μm. Super C65 structure which tends to aggregate causes the wide range in particle sizes. Conductive graphite has a size distribution that peaks at ~6 μm with a size of 0.4-20 μm. It is clear that conductive graphite is more homogeneous in size compared to Super C65.

TABLE I. The physicochemical properties of Super C65 and conductive graphite.*

Name	**BET SSA ($m^2 g^{-1}$)**	**Pore diameter (nm)**	**Particle size (μm)**
Super C65	62.060	2.735	0.2 – 600
Conductive Graphite	16.531	0.879	0.4-20

* The data were obtained from our measurement

Preparation of Si/MC/CB and Si/MC/G electrodes was accomplished by mechanical agitation of Si/MC particles, PAA, with Super C65 and conductive graphite, respectively. The morphology of the Si/MC/CB and Si/MC/G electrodes was compared by SEM analysis, as presented in Figure 2 a&b. The fresh Si/MC/CB electrode exhibits an uneven and rough surface with some Super C65 exposed on the surface (Figure 2a). The aggregates of Super C65 resulted an inhomogeneous slurry which had an impact on the morphology of the electrodes. SEM analysis was also conducted on the electrodes after cycling in order to investigate any changes in the morphology of the particles during the intercalation and de-intercalation processes. It can be seen that Si/MC/CB after cycling (Figure 2b) has some cracks and some white colored substances which can be assigned to lithium salts. The fresh Si/MC/G electrode (Figure 2c) has a more even and uniform surface than the fresh Si/MC/CB electrode. The smaller particle size range of the conductive graphite resulted a more homogeneous slurry and coating. After cycling, the Si/MC/G (Figure 2d) electrode has bigger particles and more white lithium salts. The improvement on Si/MC/CB can be explained by the chain-like, highly elastic structure of Super C65.

Further investigation of the effect of conductive additive structures on stress absorption during volume expansion and the morphology of Si/MC/CB and Si/MC/G before and after cycling was examined by TEM, presented on Figure 3 (a-d). TEM images are of a thin slice prepared via FIB cross-section. The Si/C/CB electrode before cycling (Figure 3a) presents that Si appears in dark grey with a size of 50 nm, the amorphous carbon layer in light grey and Super C65 in small dark dots. After cycling, the structure of Si/MC/CB (Figure 3b) looks amorphous, but the particles are still connected to each other. There is no big difference found on the fresh Si/MC/G electrode (Figure 3c), but small dark dots do not appear on the image. The Si/MC/G electrode after cycling (Figure 3d) has more pores and cracks. A stable SEI formed on the Si/MC/CB electrode is expected to prevent continual rupturing.

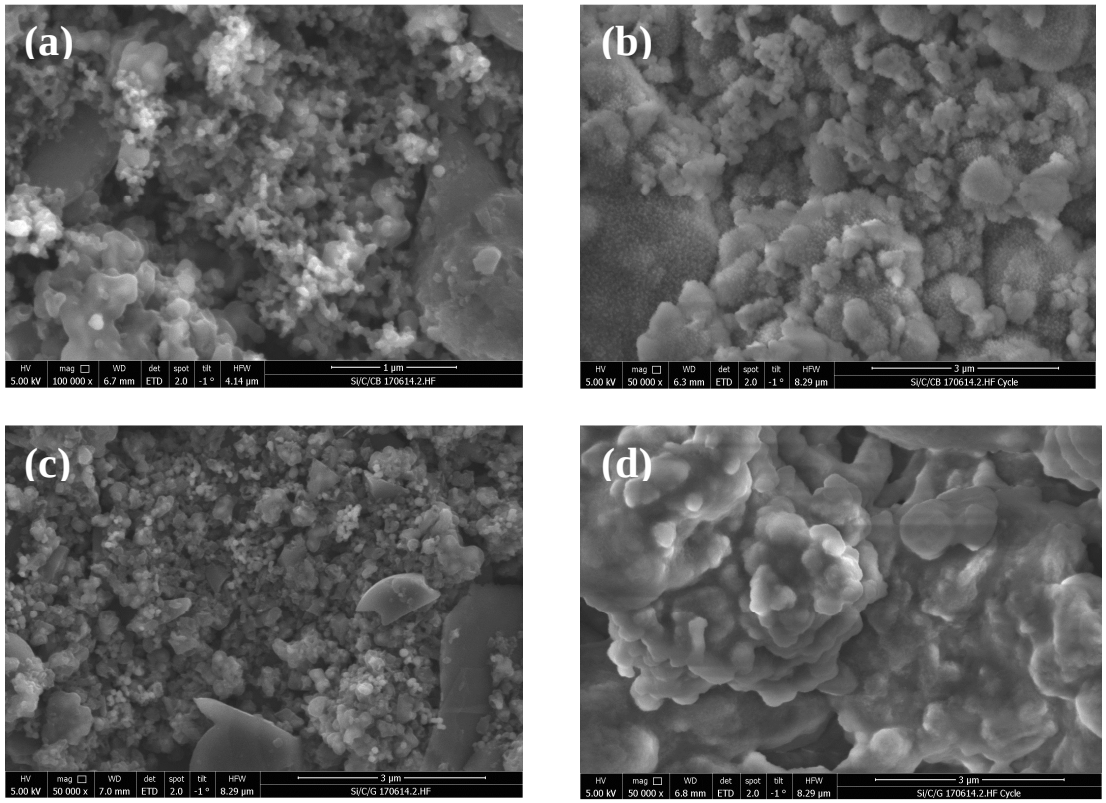

Figure 2. SEM images of the Si/MC/CB before cycling (a) and after cycling (b), Si/MC/G before cycling (c) and after cycling (d).

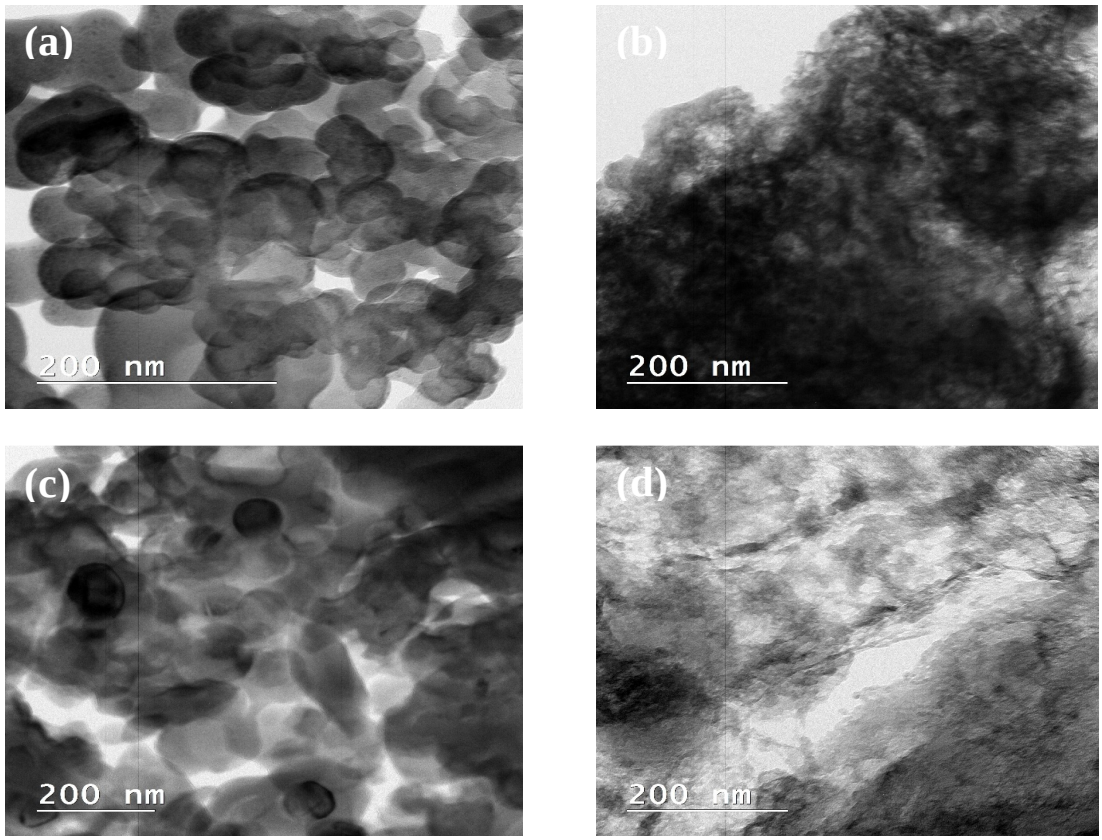

Figure 3. TEM images of a thin slice prepared via FIB cross-section of the Si/MC/CB before cycling (a) after cycling (b), Si/MC/G before etching (c) and after cycling (d).

Figure 4 shows the measured pore size distribution of the Si/MC/CB and Si/MC/G electrodes. A mean pore radius of 3.786 nm and 90.808 for Si/MC/CB, 3.845 nm and 111.620 for Si/MC/G electrodes, respectively, was obtained. Integrating the area under the curve, pore volumes of 0.244 cm^3 g^{-1} for Si/MC/CB and 0.081 cm^3g^{-1} for Si/MC/G electrodes, respectively, was obtained. The physicochemical properties of both electrodes were summarized in TABLE II. Porosity of the electrodes was calculated by dividing measured pore volume by total volume. Si/MC/CB and Si/MC/G electrodes have porosities of 16.41% and 10.16%, respectively. Both values are below the 30% which is typically applied in real cells. Lower porosity in Si/MC/G can be ascribed to the high crystallinity of conductive graphite which may cause the high compressibility of the electrodes.

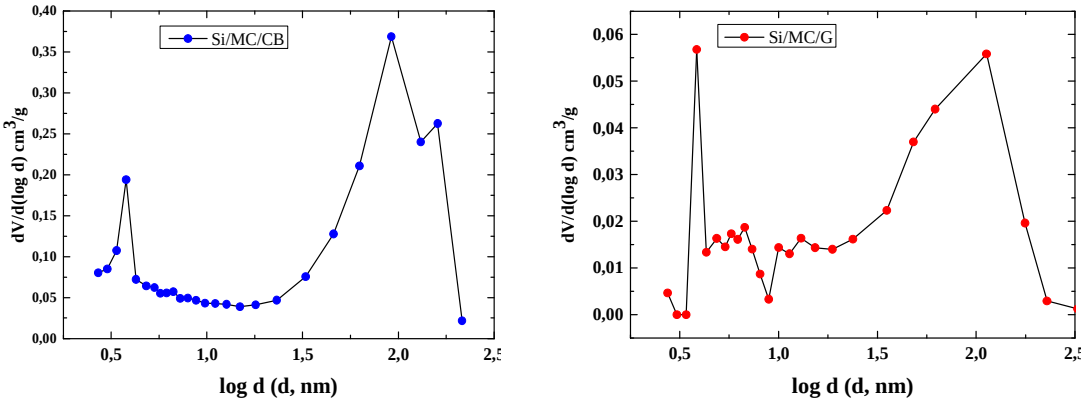

Figure 4. Pore size distribution of the Si/MC/CB and Si/MC/G electrodes.

TABLE III. The Physicochemical Properties of Si/MC/CB and Si/MC/G Electrodes.

Electrode	Mean pore size diameter (nm)	Pore volume (cm^3 g^{-1})	Porosity
Si/MC/CB	3.786 and 90.808	0.244	16.41%
Si/MC/G	3.845 and 111.620	0.081	10.16%

The electrochemical lithiation/delithiation characteristics of the electrodes were determined using cyclic voltammetry (CV). Figure **5** a-d presents CV curves for the four electrodes made from pure Super C65, pure conductive graphite, Si/MC/CB, and Si/MC/G. A broad reduction peak starting from 0.8 V vs. Li/Li^+ can be seen during first cycle and disappears in the subsequent cycles on CV of the Super C65 electrode (Figure **5**a). This peak is attributed to the formation of an SEI layer during the first cycle, in which the ethylene carbonate (EC) based electrolyte decomposition normally takes place.[18] The chemically active groups are more likely to present on the high surface area of Super C65. A broad oxidation peak at 0.2 V vs. Li/Li^+ at the following cycles corresponds to lithium intercalation. In addition, Super C65 is highly disordered with effectively a density of edge-planes which is more favorable to chemical reaction. Several differences can be seen in the CV of the graphite electrode (Figure **5**b). The SEI formation peak starting from 0.8 V vs. Li/Li^+ looks slightly weaker, which indicates less electrolyte decomposition. The low surface area of conductive graphite is beneficial in depressing SEI growth due to fewer chemically active groups, compared to Super C65. The reduction peaks at 0.15 V and 0.1 V vs. Li/Li^+ are established in conductive graphite electrode and correspond to the formation of LiC_x compounds. The sharp oxidation peaks at 0.2 and 0.25 V vs. Li/Li^+ correspond to lithium extraction. The increasing intensity

indicates the accelerated kinetics of lithiation and de-lithiation. Clearly conductive graphite is involved in the electrochemical redox process. It not only improves electronic conductivity, but also contributes to the energy density of the Si/MC electrode.

For Si/MC/CB (Figure **5**c), a strong and broad peak starting from 0.8 V vs. Li/Li^+ can be attributed to the formation of an SEI layer. The peak at 0.2 V vs. Li/Li^+ in the reduction process corresponds to the formation of Li_xSi alloys via a multi-stage mechanism while two peaks at 0.35 V and 0.5 V vs. Li/Li^+ in the oxidation process correspond to delithiation of amorphous (α) α-Li_xSi to α-Si.[7] The Si/C/G electrode (Figure **5**d) exhibited a similar broad peak starting from 0.8 V vs. Li/Li^+, corresponding to the initial formation of an SEI layer. Three reduction peaks appear at 0.25 V, 0.2 V, and 0.15 V vs. Li/Li^+ which can be attributed to the formation of LiC_x and Li_xSi. Three oxidation peaks at 0.2 V, 0.3 V, and 0.5 V vs. Li/Li^+ correspond to lithium extraction from Si nanoparticles and graphite.

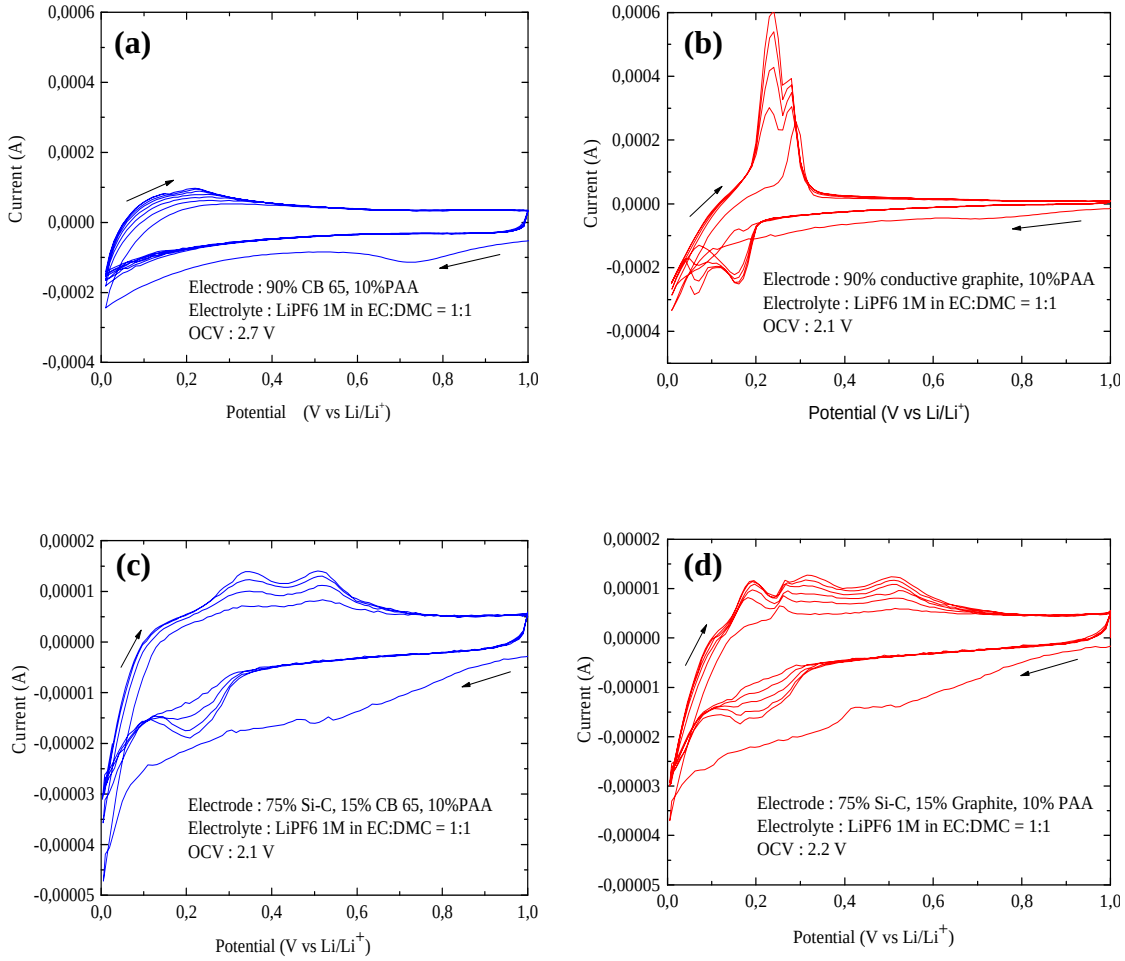

Figure 5. Cyclic voltammetry measurement of Super C65 (a), and Conductive Graphite (b) Si/MC/CB (c), Si/MC/G (d), at a scan rate of 20 μVs^{-1} over the potential window of (0.01–1)V vs. Li/Li^+.

In order to examine the cyclability performance of the electrodes, charge-discharge tests were conducted from 1 to 0.01 V with 1C rate. Figure 6 (a&b) shows the curves of gravimetric discharge capacity and coulombic efficiency versus cycle number of Si/MC/CB and Si/MC/G electrodes, respectively. The Si/MC/CB electrode (Figure 6a) reveals an initial reversible capacity of over 3521 mAh g^{-1} and coulombic efficiency of 20.60%. A significant amount of charge of 70.40% was consumed for the SEI formation which took place at potential < 0.85 V. The coulombic efficiency rapidly increased and stabilized after 50 cycles. The electrode maintains a high reversible capacity of ~ 790 mAh g^{-1} after 250 cycles with only 0,23% capacity loss per cycle. The Si/MC/G electrode reveals an initial reversible capacity of over ~4000 mAh g^{-1} and initial coulombic efficiency of 52,99%. It indicates that a less amount of charge has been consumed for SEI formation in Si/C/G compared to Si/C/CB. This result agrees well with the CV in Figure **5** (c&d). The Si/C/G maintains a reversible capacity of only 243 mAh g^{-1} after 250 cycles with 0,92 % capacity loss per cycle. The higher capacity fading from cycle to cycle is found on Si/C/G and can be assigned to a successive destruction of the Si/C/G electrode by longer cycling, which is confirmed by SEM and TEM images in Figure 2.

Coulombic efficiency (CE) is another important parameter for Si based anodes. The stable materials and SEI of Si/C/CB can afford an excellent cycle life in batteries. The stability of the SEI layer helps the Si/C/CB electrode to achieve a high CE of ~ 99.7% for 250 cycles. Super C65 which is attached at the surface of the active material can absorb and retain electrolyte. This attachment allows an intimate contact between the lithium ions and Si nanoparticles.

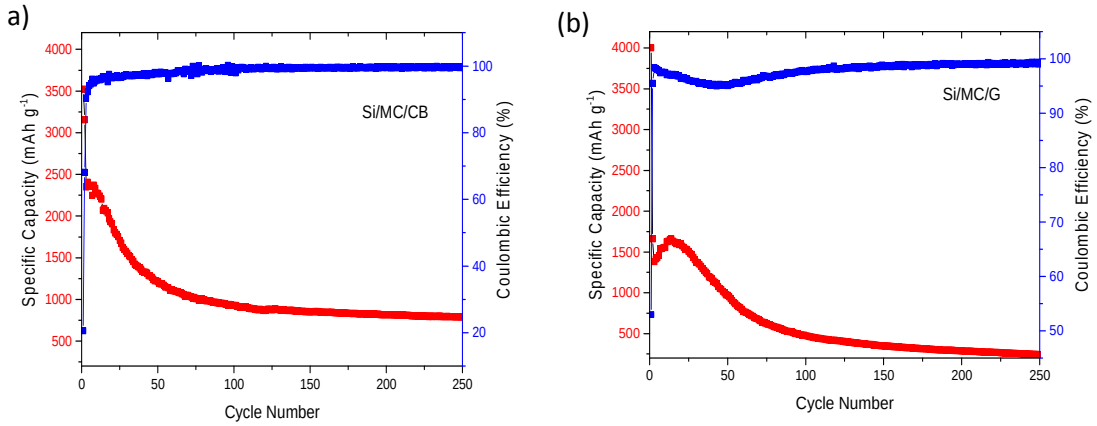

Figure 6. Electrochemical cycling performance of the Si/MC/CB (a) and Si/MC/G (b) under deep charge/discharge cycles from 1 to 0.01 V with a charge/discharge current of 1C.

To understand the electrochemical performance of Si/MC/G and Si/MC/CB electrodes, EIS has been measured after 50 and 250 cycles at 0.1 V, as presented in Figure 7. The EIS is composed of small intercept in the highest frequency region, a depressed semicircle at the medium frequency region, and a straight sloping line at the low frequency end. Such a pattern of EIS can be fitted by an equivalent circuit as shown in inset Figure 8. The small intercept corresponds to the ohmic resistance, representing the resistance of the electrolyte (Re). The semicircles appearing in the high frequency range

represent the resistance of SEI film formation (Rf). The second semicircle at low frequency range represents charge–transfer resistance (Rct) and double-layer capacitance (Cdl). The straight sloping line is related to Warburg impedance which is associated with lithium ion diffusion in the active particles. As seen in Table 4, Re of Si/MC/CB electrode is larger than in Si/MC/G, for both after 50 cycles and 250 cycles. The fitting results of each parameter are presented in Table 4. Re which is related to the ohmic drop depends on the current distribution in the electrolyte and the geometry of the electrode. The larger Re of Si/C/CB can be assigned to the less homogeneous surface. The Rf of Si/MC/G increased markedly, from 8.80 Ω to 85.1 Ω. This can be explained by the continuous formation of non-conducting SEI film on the Si/MC/G electrode. In consequence, the SEI film blocks lithium ion migration, resulting in fast capacity fade of the Si/MC/G. The Rct of Si/MC/G increases from 20.73 Ω to 62.43 Ω. The increasing Rct is probably related to the deposition of lithium ion on silicon and graphite surfaces. Si/MC/CB has less than 30% of charge transfer resistance compared to Si/MC/G, evidencing the enhanced ionic conductivity of Si/MC/CB.

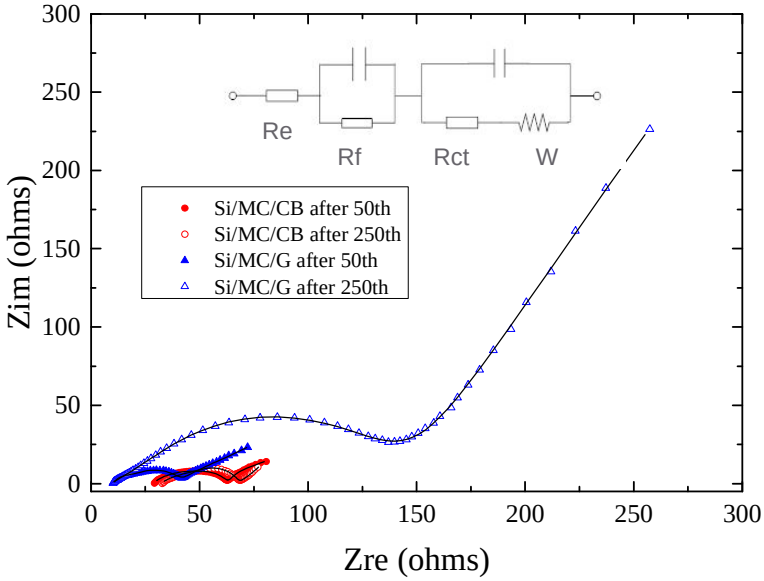

Figure 9. Nyquist plot of Si/MC/CB and Si/MC/G after 50 cycles and 250 cycles.

In addition to the electronic conductivity, high ionic conductivity is required for cell performance. Solid state diffusion and migration of lithium ions is a key to advancing Li ion batteries, known as the rate-controlling step as it restricts the rate of charge/discharge, leading to a low power output.[19] The diffusion coefficient of lithium ions (D_{Li}) was examined from the impedance data. D_{Li} can be calculated according to the following equations :

$$D_{Li} = R^2 T^2 / 2A^2 n^2 F^4 C^2_{Li} \delta^2 \quad [1]$$

Where R is the gas constant, T is the temperature, A is the surface area of the electrode, n is the number of electrons per molecule during reduction, F is the Faraday constant, C_{Li} is the concentration of lithium ions. d is the Warburg coefficient which is related to Z'.

$$Z' = Rc + Rct + \delta\, \omega^{-1/2} \quad [2]$$

Where ω is the angular frequency in the low frequency region. Both Rc and Rct are kinetics parameters independent of frequency, so δ is also the slope for the plot of Z' vs. the reciprocal square root of the low angular frequencies ($\omega^{-1/2}$). To obtain the Warburg coefficient (d), the linear fitting of Z' vs. v $\omega^{-1/2}$ in the low frequency region is done.

After 50 cycles, Si/MC/CB shows higher diffusion coefficient of lithium ions (D_{Li} = 1.11 x 10^{-12} cm^2s^{-1}) compared to Si/MC/G (D_{Li} = 9.14 x 10^{-13} cm^2s^{-1}). As well as after 250 cycles, the D_{Li} of Si/MC/CB increases (D_{Li} = 8.27 x 10^{-9} cm^2s^{-1}), higher than Si/C/G (D_{Li} = 1.11 x 10^{-12} cm^2s^{-1}). All values of the calculated diffusion coefficient of lithium ions is in the range between the diffusion coefficient of lithium ions in silicon nanoparticles and graphite which is 10^{-14}–10^{-13} cm^2s^{-1} and 10^{-11} – 10^{-9} cm^2s^{-1},[20] respectively. The higher D_{Li} in Si/MC/CB electrodes indicates faster kinetics of the cell reactions, which can be attributed to the higher porosity of the electrode. In the composite electrode, the ion diffusion is governed mostly by the pore distribution which controls electrolyte access to the active material [21].

TABLE III. EIS parameters of Si/C/CB and Si/C/G electrodes after 50 cycles and 250 cycles.

Electrode	Si/MC/CB after 50 cycles	Si/MC/CB after 250 cycles	Si/MC/G after 50 cycles	Si/MC/G after 250 cycles
Re (ohms)	28.43	31.03	10.51	9.14
Rf (ohms)	5.522	24.25	8.80	85.1
Rct (ohms)	29.74	12.05	20.73	62.43
DLi	1.11 x 10^{-12}	8.27 x 10^{-9}	9.14 x 10^{-13}	1.07 x 10^{-11}

4. Conclusions

The present work has demonstrated the impact of the selection of the conductive additive on the electrochemical performance of Si/MC anodes. Structural, morphological, and electrochemical characterization of two electrodes indicated that there were several differences between Si/MC with conductive graphite and Super C65. The morphological characterization showed that the smaller particles of Super C65 combined with the complex aggregate structure resulted Si/C/CB electrode with less homogeneous surface compared to Si/C/G electrode. Electrochemical tests showed that the highly structured conductive additive has a double function: as conductivity enhancer and active electrode component. EIS tests indicate that the Si/MC/CB has charge transfer resistance less than 30% of than that of Si/MC/G, evidencing the enhanced ionic conductivity of Si/MC/CB. In spite of its higher specific area, Super C65 presented the Si/MC electrodes with better cyclability than conductive graphite.

Acknowledgments

This work is funded by the Project EMVeM (Marie Curie Action: Initial Training Networks, "FP7-People-2012-ITN" Work Program of the European Commission). TEM

analysis was carried out using facilities as the University Service Centre for Transmission Electron Microscopy, Vienna University of Technology, Austria.

References

1. M. Armand and J. Tarascon, *Nature*, **451**, 2–7 (2008).
2. J. O. Besenhard, J. Yang, and M. Winter, *J. Power Sources*, **68**, 87–90 (1997).
3. J. Li and J. R. Dahn, *J. Electrochem. Soc.*, **154**, A156 (2007).
4. M. J. Chon, V. a. Sethuraman, A. McCormick, V. Srinivasan, and P. R. Guduru, *Phys. Rev. Lett.*, **107**, 045503 (2011).
5. I. Lahiri and W. Choi, *Crit. Rev. Solid State Mater. Sci.*, **38**, 128–166 (2013).
6. Q. Zhang, Z. Yu, P. Du, and C. Su, *Recent Pat. Nanotechnol.*, **4**, 100–110 (2010).
7. A. Magasinski et al., *Nat. Mater.*, **9**, 353–8 (2010).
8. B. Fuchsbichler, C. Stangl, H. Kren, F. Uhlig, and S. Koller, *J. Power Sources*, **196**, 2889–2892 (2011).
9. J.-G. Ren et al., *Energy Technol.*, **1**, 77–84 (2013).
10. I. A. Profatilova, C. Stock, A. Schmitz, S. Passerini, and M. Winter, *J. Power Sources*, **222**, 140–149 (2013).
11. S. L. Chou et al., *Electrochem. commun.*, **12**, 303–306 (2010).
12. L. Hu et al., *Nano Energy*, **2**, 138–145 (2013).
13. L. F. C. N. Films and L. I. Batteries, **4**, 3671–3678 (2010).
14. J. Y. Eom, J. W. Park, H. S. Kwon, and S. Rajendran, *J. Electrochem. Soc.*, **153**, A1678 (2006).
15. Y. Yao et al., *ACS Nano*, **5**, 8346–8351 (2011).
16. B. E. Warren, *J. Chem. Phys.*, **2**, 551 (1934).
17. J. R. Dahn et al., *Electrochim. Acta*, **38**, 1179–1191 (1993).
18. M. Winter, R. Imhof, F. Joho, and P. Novák, *J. Power Sources*, **81-82**, 818–823 (1999).
19. K. T. Lee and J. Cho, *Nano Today*, **6**, 28–41 (2011).
20. Y. Wang, H. Li, P. He, E. Hosono, and H. Zhou, *Nanoscale*, **2**, 1294–1305 (2010).
21. N. Ding et al., *Solid State Ionics*, **180**, 222–225 (2009).